Analytically modelling DST arrival time databases with high order polynomials for optimal high resolution imaging

Erick Baziw
Baziw Consulting Engineers Ltd., Vancouver, Canada
Gerald Verbeek
Baziw Consulting Engineers Ltd., Vancouver, Canada

ABSTRACT:

The Downhole Seismic Test (DST) is an extensively utilized geotechnical tool for site characterization. DST provides low strain ($<10^{-5}$) *in-situ* interval shear and compression wave velocity estimates. These velocities are determined by obtaining relative arrival times of source waves as they travel through the stratigraphy and are recorded by one or more vertically offset seismic sensors. The DST arrival times have associated measurements errors and resolution limitations which become more pronounced as the depth interval of analysis is reduced. The errors in arrival time measurements result in extensive fluctuations in the estimated interval velocities with numerous outliers. BCE has developed a new DST analysis technique, the so-called *DSTPolyKF* algorithm, where analytically modelling of the DST arrival time data sets is accomplished by fitting high order polynomials. The main advantages of this new technique are five-fold. 1) Ability to utilize all arrival time estimates irrespective of measurement errors. 2) Ability to process small depth interval ($\leq$ 0.5m) arrival time data sets. 3) Analytical polynomial "best fit" function allows for user specification of desired depth intervals for data interpolation. 4) Facilitates sophisticated data fusion for significantly more accurate DST interval velocity estimation. 5) Polynomial regression accuracy parameters quantify how well the "best fit" polynomial fits the acquired arrival time data sets. This paper outlines the mathematically details of the best fit polynomial where a Kalman filter formulation is implemented. The performance of the *DSTPolyKF* algorithm is demonstrated by processing real DST data sets.

1. INTRODUCTION

Downhole Seismic Testing (DST) is utilized extensively in both onshore and offshore geotechnical site investigations for the estimation of *in-situ* shear and compression wave velocities (ASTM, 2017). The shear and compression wave velocities allow for the calculation of various important geotechnical parameters such as the shear modulus, Poisson's ratio and Young's modulus. Figure 1 shows a schematic of the typical DST configuration: a seismic source is used to generate a seismic wave train at the surface. Downhole seismic receivers are used to record the seismic wave train at predefined depth increments. When triggered by the seismic source a data recording system

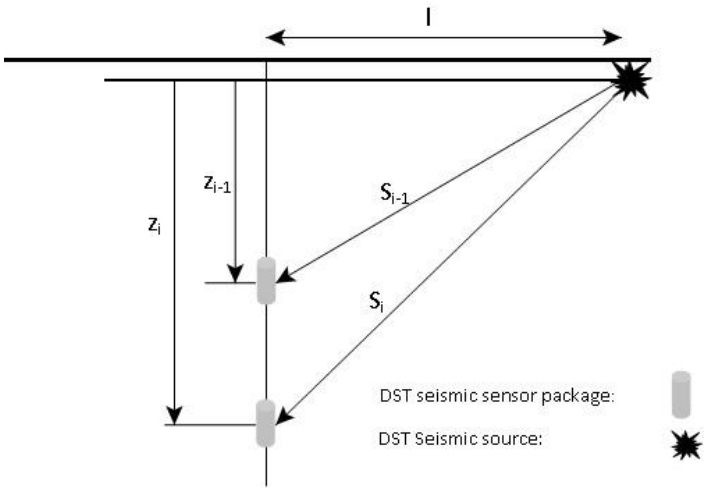

Figure 1. Schematic of the typical DST configuration.

records the response of the downhole receiver(s). Interval velocity estimates are obtained by measuring the relative and true travel times between the source waves recorded at subsequently greater depths.

In DST source wave trajectories adhere to *Fermat's principle*, which means that the raypath travels along the trajectory that minimizes the travel time between points, and that means that every depth the raypath will be different as shown in Fig.2. In Fig. 2, V_i and α_i denote the soil interval velocity and absorption, respectively. Angle θ_1 is the angle of incidence and θ_2 is called the angle of refraction. Equation (1) defines the relation between θ_1, θ_2, V_1 and V_2.

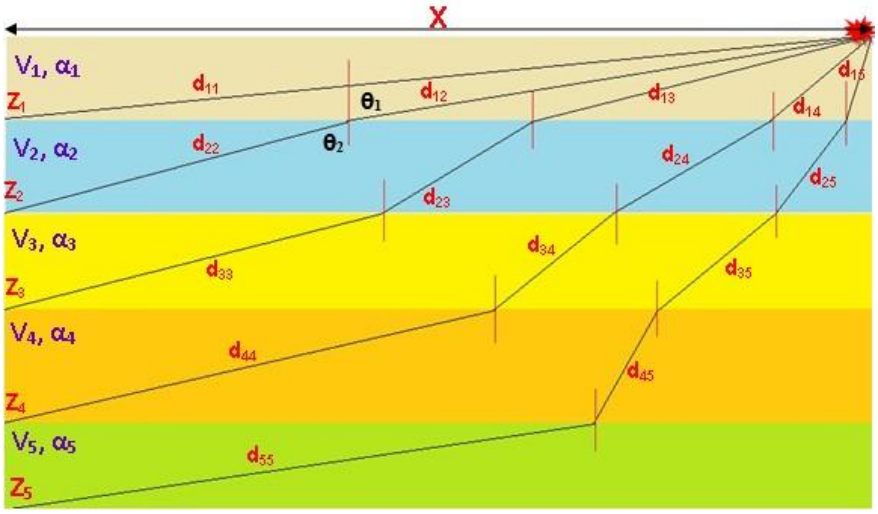

Figure 2. Schematic of thin layer effect for a sand layer embedded in a clay layer (Baziw and Verbeek, 2021).

Equation 1 is referred to as *Snell's Law* (Aki and Richards (2002)) and is derived from *Fermat's Principle*, which states that a wave will take that raypath for which the travel time is stationary with respect to minor variations of the raypath (Shearer, 1999).

$$Sin\ \theta_1 / V_1 = Sin\ \theta_2 / V_2 = p \qquad (1)$$

quantity p is called the raypath parameter.

Baziw and Verbeek (Baziw, 2002; Baziw and Verbeek, 2012, 2019, 2021a) have developed a methodology, the so called Forward Modelling Downhill Simplex Method (FMDSM), which implements *Fermat's Principle* when processing DST data sets.

There are several factors which can lead to DST arrival time measurement errors. These measurement errors are predominantly due to poor data quality, low resolution of the seismic sensor and corresponding small DST depth increments, and the type of data trigger utilized. Poor quality DST seismic data recordings general results from "dirty" sources (e.g., poor coupling between seismic hammer plate and soil), poor sensor-stratigraphy coupling, complicated stratigraphy resulting in source wave reflections, refraction etc., and insufficient energy output of the seismic source.

The two types of seismic sensors utilized in DST for acquiring seismic source waves are geophones and accelerometers. On rare occasions (e.g., saturated borehole) hydrophones are utilized. Ideally the seismic sensor should provide signals which are unaffected by the sensors inherent characteristics and as closely as possible reflect the true soil response to the seismic source wave traveling through it and ambient measurement noise (i.e., input = output). In terms of frequency response of the receiver, its output should be constant for all input frequencies. In addition, the phase of the input frequency should be unaffected so that the wave's shape does not change (Baziw et al., 2000). In general terms it is desirable to have a seismic sensor with a fast response time and a small settling time. high precision piezoelectric accelerometers (operational amplifier integrated into sensor) are preferable due to their low noise, fast response times, and high

bandwidths compared to geophones. High precision accelerometers typically have desirable rise and decay times (in the order of 5 μs), and these characteristics ensure recorded traces with minimal or no sensor distortion (input = output). For these reasons, DTS investigations with relative small depth increments should utilize high precision accelerometers.

In DST there are two types of trigger mechanisms: 1) *contact* triggers whereby the system is triggered when contact is made between source and receiver (e.g., when the source hammer strikes the plate), and 2) *sensor* triggers when the signal of a transducer (e.g. an accelerometer or geophone) is used to trigger the system. *contact* triggers are significantly more accurate than *Sensor* triggers. This is due to the fact that c*ontact* triggers have a very low noise environment and very fast rise time when contact is made. The c*ontact* trigger ensures a very accurate reference trigger time.

To address the outlined DST measurement errors, BCE has developed a new DST analysis technique, the so-called *DSTPolyKF* algorithm, which "best fits" a high order polynomial to arrival time data sets. This technique implements a Kalman filter formulation so that arrival time data sets can be processed sequentially with measurement errors assigned for each estimated arrival time (allowing for variable weight on arrival time estimates); Furthermore, the KF is an ideal mathematical tool for data fusion. In this case numerous and relevant data sets are utilized for optimal estimation of desired parameters.

2. MATHEMATICAL BACKGROUND AND *DSTPolyKF* ALGORITHM FORMULATION

2.1 Kalman Filter

The Kalman Filter (KF) is a Bayesian Recursive Estimation (BRE) filtering technique based on state-space, time-domain formulations of physical problems (Gelb, 1974; Arulampalam et al., 2002; Baziw, 2007; Baziw and Verbeek, 2021b). Application of this filter type requires that the dynamics of the system and measurement model, which relates the noisy measurements to the system state equations, be describable in a mathematical representation and probabilistic form that uniquely define the system behaviour. Baziw and Verbeek (2021b) give a detailed outline of the KF governing equations and the implementation of these equations. The Kalman Filter (KF) equations are outlined in Table 1.

In Table 1 $\boldsymbol{x_k}$ denotes the state to be estimated, $\boldsymbol{F}_{k-1}$denotes the state transition matrix which describes the system dynamics, $\boldsymbol{u}_{k-1}$ the process or system noise (model uncertainty), $\boldsymbol{G}_{k-1}$ describes the relationship between $\boldsymbol{x_k}$ and $\boldsymbol{u}_{k-1}$, and $\boldsymbol{H}_k$ the relationship between the state and the available measurement (source wave

Table 1
KF Governing Equations

DESCRIPTION	Mathematical Representation	Eq.
System equation	$x_k = F_{k-1}x_{k-1} + G_{k-1}u_{k-1}$	2
Measurement equation	$z_k = H_k\, x_k + v_k$	3
State estimate extrapolation	$\hat{x}_{k\|k-1} = F_{k-1}\hat{x}_{k-1\|k-1}$	4
Error covariance extrapolation	$P_{k\|k-1} = F_{k-1}P_{k-1\|k-1}F_{k-1}^{T} + G_{k-1}Q_{k-1\|k-1}G_{k-1}^{T}$	5
Measurement extrapolation	$\hat{z}_k = H_{k-1}\hat{x}_{k\|k-1}$	6
Innovation	$\Delta_k = z_k - \hat{z}_k$	7
Variance of innovation	$S_k = H_k\, P_{k\|k-1}H_k^T + R_k$	8
Kalman gain matrix	$K_k = P_{k\|k-1}H_k(S_k)^{-1}$	9
State estimate update	$\hat{x}_{k\|k} = \hat{x}_{k\|k-1} + K_k\, \Delta_k$	10
Error covariance update	$P_{k\backslash k} = [I - K_k\, H_k\,]P_{k\|k-1}$	11

In (2) and (3) $\boldsymbol{v}_k$ and $\boldsymbol{u}_k$ are *i.i.d* Gaussian zero mean white noise processes with variances of $\boldsymbol{Q}_k$ and $\boldsymbol{R}_k$, respectively (i.e.,$v_k \sim N(0, R_k)$ and $u_k \sim N(0, Q_k)$).

arrival time). The KF can be applied to problems with linear time-varying systems and with non-stationary system and measurement statistics. Problems with nonlinearities are handled by linearizing the system and measurement equations. The Kalman Filter is readily applied to estimation, smoothing and prediction.

2.2 DSTPolyKF Algorithm Formulation

2.2.1 Polynomial Regression and the Assessment of its Accuracy

Polynomial regression is a commonly utilized technique for analytically modelling data sets with measurement errors. The polynomial regression equation is given as

$$z_k = \hat{z}_k + v_k = a_0 + a_1 d + a_2 d^2 + a_3 d^3 + a_4 d^4 + \cdots + a_n d^n + v_k \quad (12)$$

where $\hat{z}_k$ is the polynomial regression estimator, n is the degree of the polynomial, v_k is the measurement error and $d = k\Delta$, Δ is the sampling rate.

Ostertagová, (2012) outlines four parameters which can be utilized to evaluate the accuracy of the polynomial regression best fit. These four parameters are mean squared error (MSE) of the polynomial estimator, Mean Absolute Percentage Error (MAPE), coefficient of determination (R^2), and adjusted coefficient of determination (R^{*2}). Table 2 outlines the four polynomial regression accuracy parameters by their mathematical representations and important characteristics. In the *DSTPolyKF* algorithm polynomial regressions of order 2 to 7 are derived for the estimated DST source wave arrival times. The polynomial aggression order[1] which results in the "best" accuracy parameter values as defined in Table 2 and lowest polynomial order is utilized. This approach addresses the well-known bias-variance tradeoff of polynomial regression (Emmert-Streib and Dehmer, 2019).

2.2.2 DSTPolyKF algorithm state-space formulation and measurement model

n^{th} Degree Polynomial Measurement Model

The following states need to be defined for estimating the n^{th} degree polynomial coefficients outlined in eq. (12) with a KF

[1] The maximum number of turnings of a polynomial function is always one less than the degree

$$\begin{bmatrix} x_1 \\ x_2 \\ x_3 \\ x_4 \\ \vdots \\ x_{n-1} \\ x_n \\ x_{n+1} \end{bmatrix} \equiv \begin{bmatrix} a_0 \\ a_1 \\ a_2 \\ a_3 \\ \vdots \\ a_{n-2} \\ a_{n-1} \\ a_n \end{bmatrix} \quad (17)$$

Table 1. Polynomial regression best fit accuracy parameters

Parameter and Mathematical Equation		**Notes**
$MSE = \frac{SSR}{df_E} = \frac{\sum_{k=1}^{m}(z_k - \hat{z}_k)^2}{m-(n+1)}$ SSR is the Sum of Squares Residual. The SSR has χ^2 distribution with $df_E = m-(n+1)$ degrees of freedom.	(13)	MSE is an unbiased estimator of the variance of the measurement error. Parameter RMSE is the Root Mean Square Error where RMSE = √MSE. RMSE is a biased estimator of the standard deviation of the measurement error.
$MAPE = \frac{100}{m}\sum_{k=1}^{m}\left\|\frac{z_k - \hat{z}_k}{z_k}\right\|$	(14)	MAPE measures relative performance or prediction accuracy of a forecasting method in statistics. MAPE values and the associated prediction accuracy are outline in below.

MAPE Value	**Prediction Accuracy**
MAPE<10%	excellent
10% ≤ MAPE ≤ 20%	good
20% < MAPE ≤ 50%	acceptable
50% < MAPE	inaccurate

$R^2 = 1 - \frac{SSR}{TSS} = 1 - \frac{\sum_{k=1}^{m}(z_k - \hat{z}_k)^2}{\sum_{k=1}^{m}(z_k - \bar{z})^2}$ $\bar{z}$ is the arithmetic mean. TSS is the Total Sum of Squares.	(15)	R^2 measures how the percentage of variation in variable z_k can be explained by the explanatory variable d in eq. (12). In general terms, R^2 quantifies what percentage of the measured z_k values reside on the best fit polynomial $\hat{z}_k$. R^2 is similar to the correlation coefficient. The correlation coefficient quantifies how strong of a linear relationship there is between two variables. R^2 values and the associated prediction accuracy are outline below. **R^2 value** / **Prediction Accuracy** $0.9 \leq R^2$ — excellent $0.8 \leq R^2 < 0.9$ — good $0.6 \leq R^2 < 0.8$ — acceptable $R^2 < 0.6$ — inaccurate
$R^{*2} = R^2 - \frac{(1 - R^2)n}{m - (n + 1)}$	(16)	R^{*2} is the adjusted value of the coefficient of determination in which the order of the polynomial is taken into account. Prediction accuracy is poor if R^{*2} is significantly lower than R^2.

The discrete system equation (eq. (2)) is given as

$$\begin{bmatrix} x_{1k+1} \\ x_{2k+1} \\ x_{3k+1} \\ x_{4k+1} \\ \vdots \\ x_{(n-1)k+1} \\ x_{(n)k+1} \\ x_{(n+1)k+1} \end{bmatrix} = \begin{bmatrix} 1 & 0 & 0 & 0 & 0 & 0 & 0 & 0 \\ 0 & 1 & 0 & 0 & 0 & 0 & 0 & 0 \\ 0 & 0 & 1 & 0 & 0 & 0 & 0 & 0 \\ 0 & 0 & 0 & 1 & 0 & 0 & 0 & 0 \\ 0 & 0 & 0 & 0 & \ddots & 0 & 0 & 0 \\ 0 & 0 & 0 & 0 & 0 & 1 & 0 & 0 \\ 0 & 0 & 0 & 0 & 0 & 0 & 1 & 0 \\ 0 & 0 & 0 & 0 & 0 & 0 & 0 & 1 \end{bmatrix} \begin{bmatrix} x_{1k} \\ x_{2k} \\ x_{3k} \\ x_{4k} \\ \vdots \\ x_{(n-1)k} \\ x_{nk} \\ x_{(n+1)k} \end{bmatrix} \tag{18}$$

The linear measurement matrix, H, is given by the following equation

$$H_k = [1 \quad d \quad d^2 \quad d^3 \quad \cdots \quad d^{n-3} \quad d^{n-2} \quad d^{n-1}] \tag{19}$$

3. *DSTPolyKF* ALGORITHM PERFORMANCE ASSESSMENT

The *DSTPolyKF* algorithm was implemented on both onshore and offshore challenging DST arrival time data sets for performance assessment of the algorithm. The onshore DST data sets had SH source waves generated on both the Right Side (RS) and Left Side (LS) of the downhole seismic probe resulting in two source wave traces recorded for each depth increment. The onshore

DST instrumentation utilized high precision triaxial accelerometers and contact triggers. The offshore investigation also generated both RS and LS SH source waves. In this case both "top" and "bottom" triaxial sensor arrangement packages were utilized. This resulted in four source wave traces for each depth increment. The Top Sensor (TS) and Bottom Sensor (BS) were vertically offset by 1m. The offshore DST instrumentation utilized geophone sensors and a geophone sensor trigger.

3.1 Onshore Data Analysis

Figure 3 illustrates the estimated LS and RS estimated arrival times for the onshore DST data set. As is illustrated in Fig. 3, there is significant variability between the LS and RS arrival estimates from 12m to 21m. This results in significant variability in the resulting interval velocity estimates. Table 3 outlines the corresponding polynomial regression estimated accuracy parameters for the averaged arrival times (LS and RS) illustrated in Fig. 3 and orders 2 to 7. From the results outlined in Table 3, the 6th and 7th order polynomial aggressions have overall "best" accuracy parameter values as defined in Table 2. Figure 4 illustrates the averaged LS and RS arrivals times with the 7th order polynomial regression best fit line. Figure 5 illustrates the FMDSM output with source wave raypaths illustrated when processing the 7th order best fit polynomial regression arrival times. Table 4 outlines the estimated interval velocities and percent differences for polynomial regressions of orders 6 and 7. The 6th and 7th order percent differences are below the desired 10% for the all depths except 18.5, 19m, 19.5m (just exceeding 10%). The estimate at 21m should be dropped due to the large percent difference. In general terms, when comparing polynomial regression of varying orders with similar "best" accuracy parameters the discrepancies of velocity estimates occurred at the end of the polynomial regression best fit lines. Figure 6 illustrates the 7th order best fit polynomial regression interval velocity plot with an interpolated 0.25m depth increment and the interval velocity estimate at 21m dropped.

Table 3. Estimated polynomial accuracy parameters for offshore data analysis

Polynomial Order	RMS	MAPE	R^2	R^{*2}
2	6.0434	7.9976	0.99727	0.996966
3	3.9483	4.9092	0.998899	0.998705
4	1.9703	2.0815	0.999742	0.999678
5	1.8957	1.5455	0.999776	0.999702
6	1.7769	1.4371	0.999816	0.999738
7	1.6805	1.5168	0.999848	0.999765

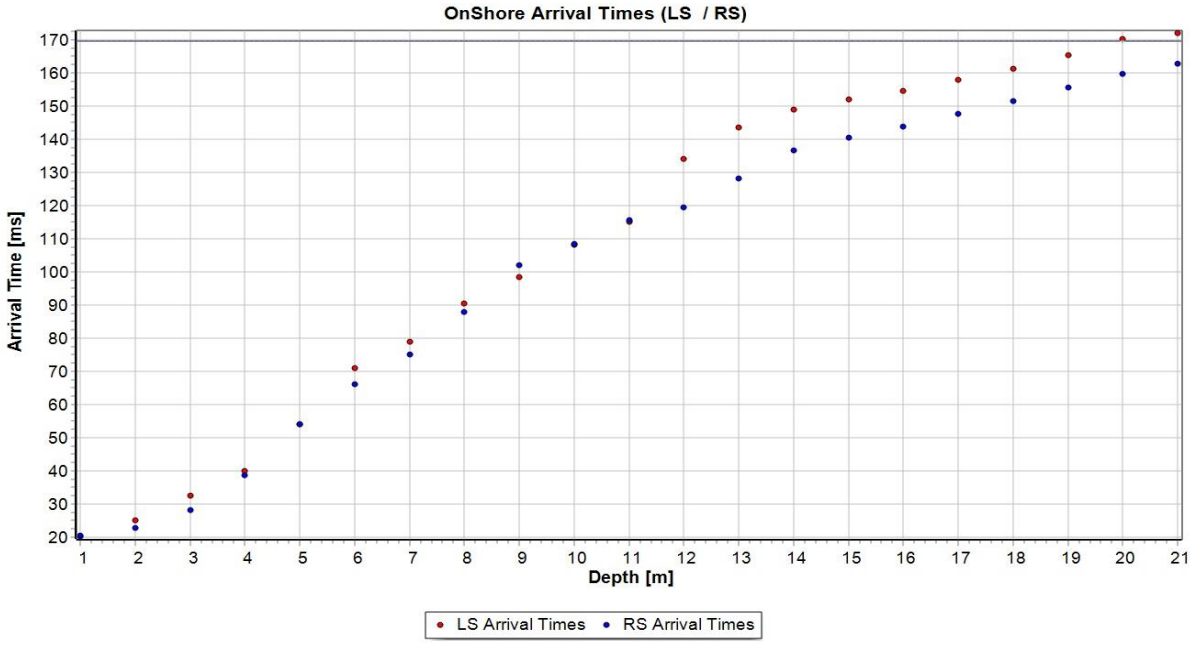

Figure 3. LS and RS arrival times for the onshore real DST analysis.

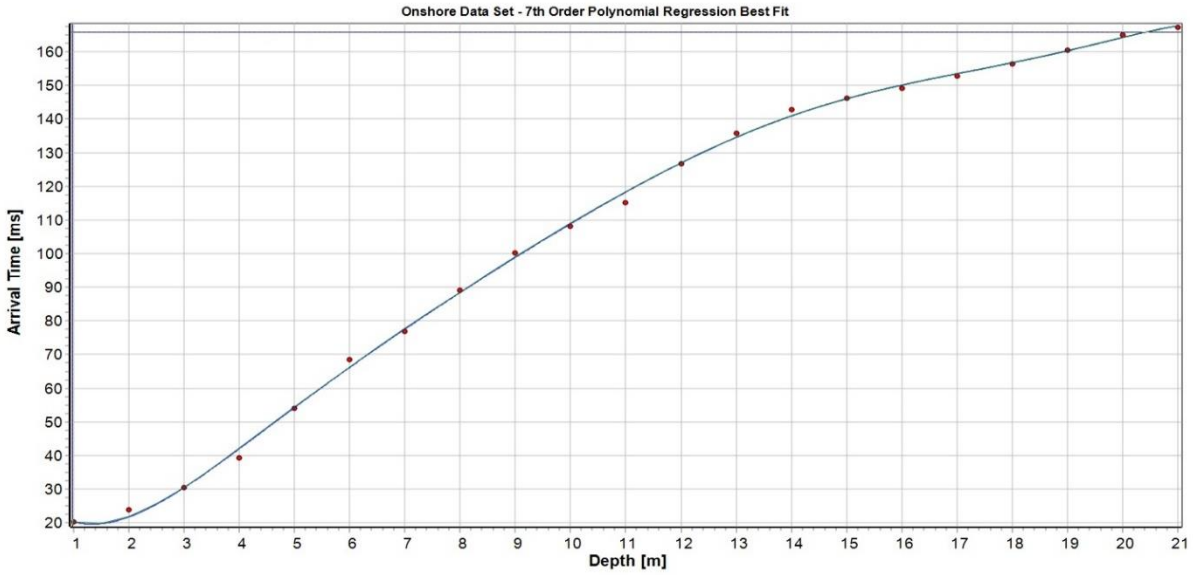

Figure 4. Averaged arrival times (red dots) and 7th order polynomial regression best fit (blue line) for the onshore real DST analysis.

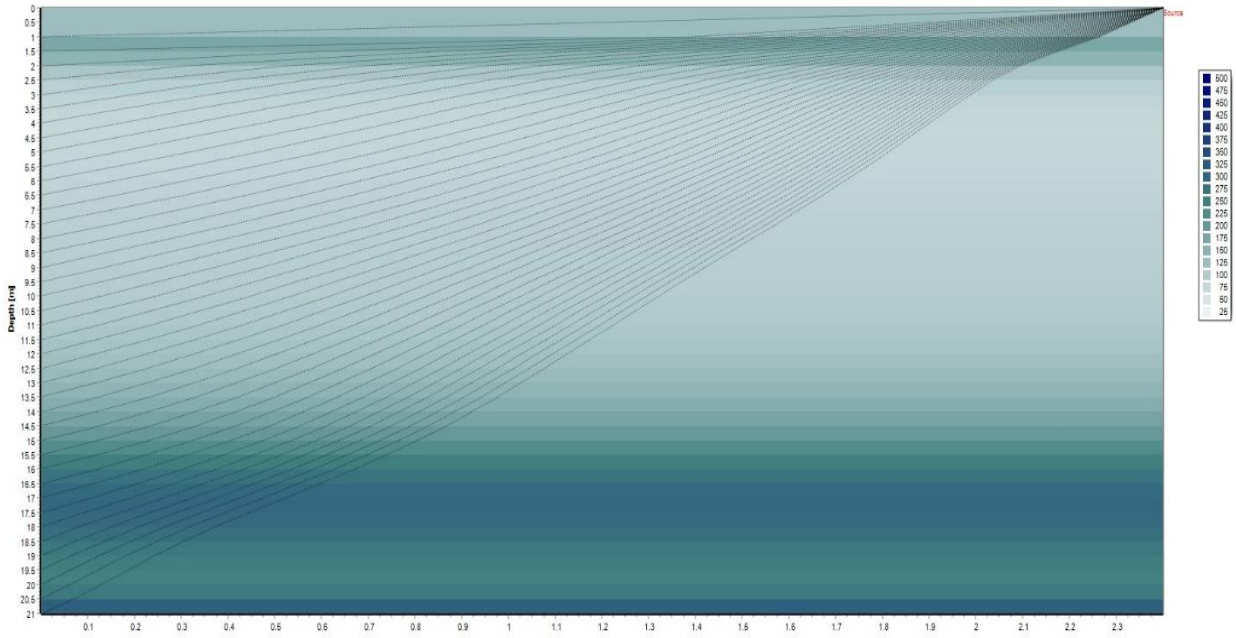

Figure 5. FMDSM output with source wave raypaths (black lines) illustrated when processing the 7th order best fit polynomial regression arrival times shown in Fig. 4.

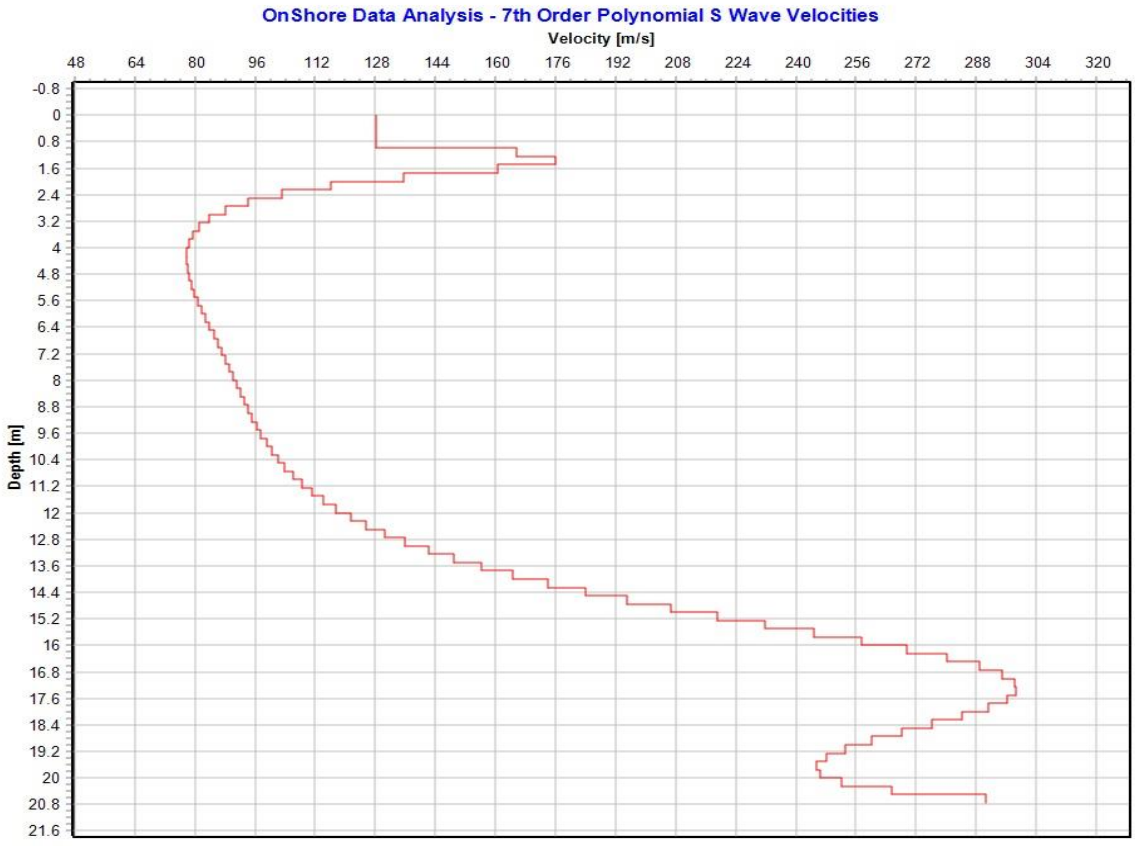

Figure 6. 7th order best fit polynomial regression interval velocity plot with an interpolated 0.25m depth increment and the estimate at 21m dropped for the onshore data set.

Table 4. Estimated interval velocities and percent differences for polynomial regressions of orders 6 and 7.

Depth [m]	6th Order Interval Velocity [m/s]	7th Order Interval Velocity [m/s]	6th and 7th Order Precent difference
1	128.3	128.3	0
1.5	151.2	171.1	6.2
2	136.9	147.8	3.8
2.5	113.8	109.3	2
3	98.1	91	3.8
3.5	88.5	82.4	3.6
4	82.7	78.5	2.6
4.5	79.5	77.3	1.4
5	77.9	77.8	0.1
5.5	77.6	79.2	1
6	78.2	81.2	1.9
6.5	79.6	83.4	2.3
7	81.6	85.7	2.5
7.5	84	87.9	2.3
8	86.9	89.9	1.7
8.5	90.1	91.9	1
9	93.6	93.9	0.2
9.5	97.5	96	0.8
10	101.6	98.4	1.6
10.5	106	101.4	2.2
11	110.7	105.1	2.6
11.5	116	109.8	2.7
12	121.7	115.9	2.4
12.5	128.2	123.5	1.9
13	135.6	133.2	0.9
13.5	144.2	145.3	0.4
14	154.4	160.3	1.9
14.5	166.6	178.6	3.5
15	181.2	200.2	5
15.5	199	224.7	6.1
16	220.7	250.4	6.3
16.5	246.5	274.1	5.3
17	276.5	291.3	2.6
17.5	308.9	298.2	1.8
18	338.9	293.7	7.1
18.5	357.9	280.6	12.1
19	355.1	264.5	14.6
19.5	325.5	251.1	12.9
20	275.6	246.4	5.6
20.5	219.3	259	8.3
21	168.1	312.7	30.1

3.2 Offshore Onshore Data Analysis

Figure 7 illustrates the estimated (Top Sensor LS) TSLS, TSRS (Top Sensor RS), BSLS (Bottom Sensor LS) and BSRS (Bottom Sensor RS) estimated arrival times for the offshore DST data set. Table 5 outlines the corresponding polynomial regression estimated accuracy parameters for the averaged arrival times (TSLS, TSRS, BSLS, and BSRS) illustrated in Fig. 7 and orders 2 to 7. From the results outlined in Table 5, the 6th and 7th order polynomial aggressions have overall "best" accuracy parameter values as defined in Table 2. Although, the 5th order polynomial regression result are also very close to 6th and the 7th order polynomial results. Figure 8 illustrates the averaged TSLS, TSRS, BSLS and BSRS arrivals times with the 7th order polynomial regression best fit line. Figure 9 illustrates the FMDSM output when processing the 7th order best fit polynomial regression arrival times. Table 6 outlines the estimated interval velocities and percent differences for polynomial regressions of orders 6 and 7. Figure 10 illustrates the 7th order best fit polynomial regression interval velocity plot with an interpolated 0.5m depth.

Table 5. Estimated polynomial accuracy parameters for offshore data analysis

Polynomial Order	RMS	MAPE	R^2	R^{*2}
2	4.8413	4.2236	0.998327	0.998264
3	2.4921	1.9924	0.999565	0.99954
4	1.2825	1.0099	0.999887	0.999878
5	1.0571	0.7638	0.999925	0.999917
6	1.0357	0.6924	0.999929	0.999921
7	0.9672	0.6404	0.99994	0.999931

CONCLUSIONS

Downhole Seismic Test (DST) DST provides low strain ($<10^{-5}$) *in-situ* interval shear and compression wave velocity estimates. These velocities are determined by obtaining arrival times of source waves as they travel through the stratigraphy and are recorded by one or more vertically offset seismic sensors. There are several factors which can lead to DST arrival time measurement errors. These measurement errors are predominantly due to poor data quality, low resolution of the seismic sensor and corresponding small DST depth increments, and the type of data trigger utilized. Poor quality DST seismic data recordings general results from "dirty" sources (e.g., poor coupling between seismic hammer plate and soil), poor sensor-stratigraphy coupling, complicated stratigraphy resulting in source wave reflections, refraction etc., and insufficient energy output of the seismic source. This paper has outlined a new analysis technique, the so-called *DSTPolyKF* algorithm, where analytically modelling of the DST arrival time data sets is accomplished by fitting high order polynomials. The main advantages of this new technique are five-fold. 1) Ability to utilize all arrival time estimates irrespective of measurement errors. 2) Ability to process small depth interval ($\leq$ 0.5m) arrival time data sets. 3) Analytical polynomial "best fit" function allows for user specification of desired depth intervals for data interpolation. 4) Facilitates sophisticated data fusion for significantly more accurate DST interval velocity estimation. 5) Polynomial regression accuracy parameters quantify how well the "best fit" polynomial fits the acquired arrival time data sets. This paper has described the mathematically details of the *DSTPolyKF* algorithm where four best fit polynomial regression accuracy parameters were outlined. In addition, the performance of the *DSTPolyKF* algorithm was demonstrated by processing real DST data sets from both onshore and offshore investigations.

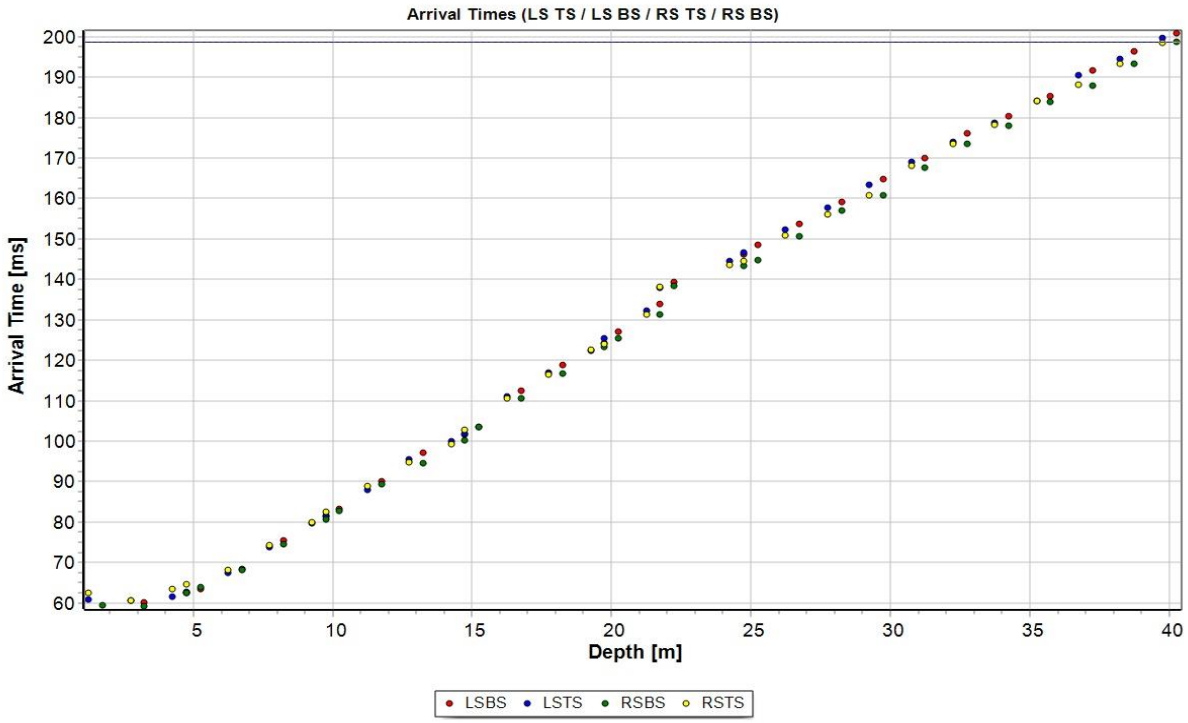

Figure 7. TS LS, TS RS, BS LS and BS RS arrival times for the offshore real DST analysis.

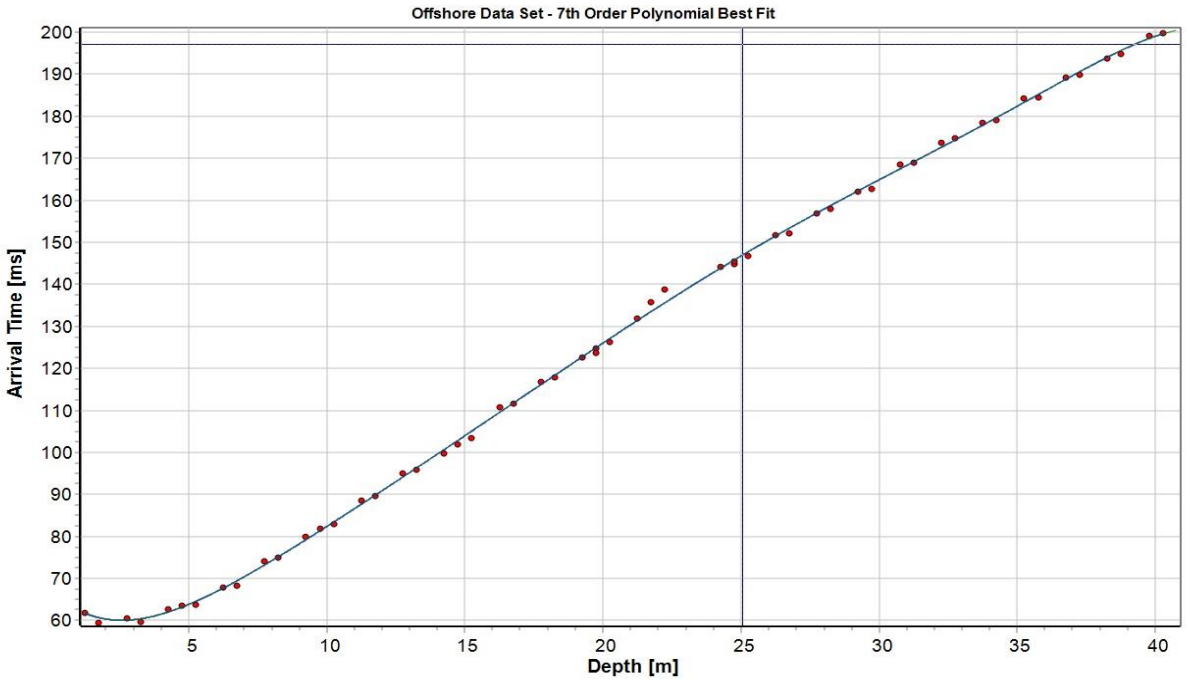

Figure 8. Averaged arrival times (red dots) and 7th order polynomial regression best fit (blue line) for the offshore real DST analysis.

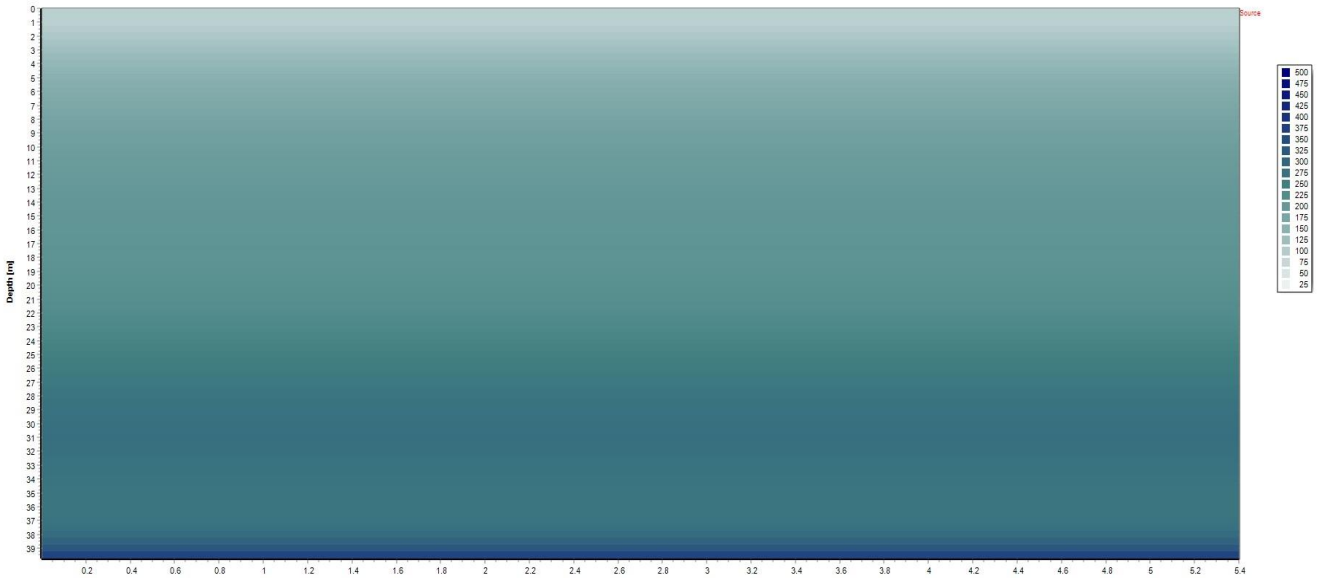

Figure 9. FMDSM output when processing the 7th order best fit polynomial regression arrival times shown in Fig. 8.

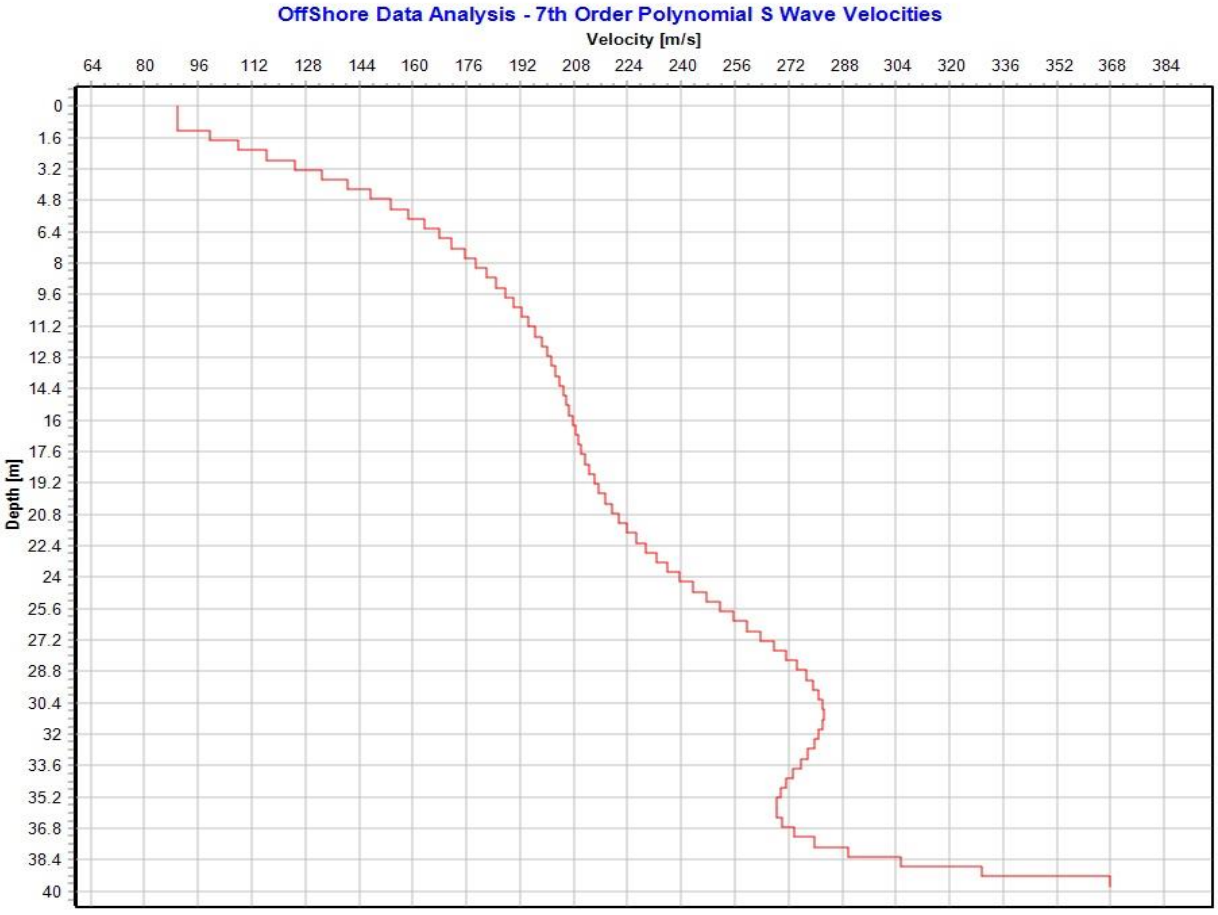

Figure 10. 7th order best fit polynomial regression interval velocity plot with an interpolated 0.5m depth increment for the offshore data set.

Table 6. Estimated interval velocities and percent differences for polynomial regressions of orders 6 and 7.

Depth [m]	6^{th} Order Interval Velocity [m/s]	7^{th} Order Interval Velocity [m/s]	6^{th} and 7^{th} Order Precent difference
1.24	89.7	89.7	0
1.74	98.3	99.6	0.7
2.24	105.9	108	1
2.74	114.2	116.5	1
3.24	123.1	125	0.8
3.74	132.3	133.1	0.3
4.24	141.2	140.6	0.2
4.74	149.6	147.3	0.8
5.24	157.1	153.3	1.2
5.74	163.7	158.7	1.6
6.24	169.1	163.4	1.7
6.74	173.5	167.8	1.7
7.24	177	171.7	1.5
7.74	179.8	175.4	1.2
8.24	181.9	178.8	0.9
8.74	183.6	181.9	0.5
9.24	185	184.8	0.1
9.74	186.2	187.6	0.4
10.24	187.4	190.1	0.7
10.74	188.5	192.4	1
11.24	189.7	194.6	1.3
11.74	190.9	196.6	1.5
12.24	192.2	198.4	1.6
12.74	193.7	200	1.6
13.24	195.3	201.4	1.5
13.74	196.9	202.7	1.5
14.24	198.7	203.8	1.3
14.74	200.6	204.9	1.1
15.24	202.5	205.8	0.8
15.74	204.6	206.7	0.5
16.24	206.7	207.6	0.2
16.74	208.8	208.4	0.1
17.24	211	209.3	0.4
17.74	213.3	210.3	0.7
18.24	215.5	211.4	1
18.74	217.8	212.6	1.2
19.24	220.1	214	1.4
19.74	222.3	215.5	1.6
20.24	224.6	217.2	1.7
20.74	226.8	219.2	1.7
21.24	229.1	221.4	1.7
21.74	231.3	223.8	1.6
22.24	233.5	226.5	1.5
22.74	235.6	229.4	1.3
23.24	237.8	232.6	1.1
23.74	239.9	236	0.8
24.24	242	239.7	0.5
24.74	244.1	243.5	0.1
25.24	246.2	247.4	0.2

25.74	248.3	251.5	0.6
26.24	250.5	255.7	1
26.74	252.6	259.8	1.4
27.24	254.8	263.8	1.7
27.74	257	267.7	2
28.24	259.2	271.2	2.3
28.74	261.5	274.5	2.4
29.24	263.8	277.2	2.5
29.74	266.1	279.5	2.5
30.24	268.5	281.1	2.3
30.74	270.9	282.1	2
31.24	273.4	282.4	1.6
31.74	275.9	282.1	1.1
32.24	278.3	281.1	0.5
32.74	280.7	279.7	0.2
33.24	283.1	277.8	0.9
33.74	285.4	275.6	1.7
34.24	287.5	273.4	2.5
34.74	289.4	271.3	3.2
35.24	291.1	269.6	3.8
35.74	292.4	268.6	4.2
36.24	293.3	268.6	4.4
36.74	293.8	270.1	4.2
37.24	293.7	273.6	3.5
37.74	292.9	279.8	2.3
38.24	291.3	289.9	0.2
38.74	289	305.5	2.8
39.24	285.7	329.7	7.1
39.74	281.4	368	13.3

REFERENCES

[1] Aki, K. and Richards, P.G. (2002), Quantitative Seismology, 2nd edition, Sausalito, California: University Science Books. pp. 88-89.

[2] Arulampalam, M.S., Maskell, S., and Clapp, T. (2002), “A tutorial on particle filters for online nonlinear/nonGaussian Bayesian tracking”, IEEE Transactions on Signal Processing, vol. 50, no. 2, pp. 174-188, Feb. 2002

[3] ASTM D6067 / D6067M – 17 (2017), “Standard Practice for Using the Electronic Piezocone Penetrometer Tests for Environmental Site Characterization and Estimation of Hydraulic Conductivity”, ASTM Vol. 4.09 Soil and Rock (II): D5877-latest.

[4] Baziw, E., Tichy, J, and de Caprona, G (2000),"Data Acquisition in Seismic Cone Penetration Testing". In Proceedings of the 3rd International Symposium on Integrated Technical Approaches to Site Characterization (ITASCE), Argonne, IL, 11 14 Sept. 2000. Argonne National Laboratory. pp. 69-72.

[5] Baziw, E. (2007), Application of Bayesian Recursive Estimation for Seismic Signal Processing, Ph.D. Thesis, Dept. of Earth and Ocean Sciences, University of British Columbia.

[6] Baziw, E. (2002), "Derivation of Seismic Cone Interval Velocities Utilizing Forward Modeling and the Downhill Simplex Method", Can. Geotech. J., 39(5), pp.1181-1192.

[7] Baziw, E., and Verbeek, G. (2012), “Deriving Interval Velocities from Downhole Seismic Data”, Geotechnical and Geophysical Site Characterization 4 – Mayne (eds), CRC Press, 1019–1024.

[8] Baziw, E. and Verbeek, G. (2019), " Unique algorithm which takes into account source wave travel paths when estimating absorption values from DST data sets" published in the DFI 44rd Annual Conference on Deep Foundations conference proceedings. October 14-17, 2019 - Chicago, IL.

[9] Baziw, E., and Verbeek, G. (2021a), “Implementation of the FMDSMAA algorithm” published in the conference proceedings of the 6th International Conference on Geotechnical Site Characterization (ISC-6), Budapest – Hungary, September 26-29, 2021.

[10]Baziw, E. and Verbeek, G. (2021b), "Implementation of Kalman Filtering Techniques for Filtering CPT Cone Bearing Measurements", published in the DFI 46th Annual Conference on Deep Foundations conference proceedings. October 12-15, 2021 - Las Vegas, NV.
[11]Emmert-Streib, F. and Dehmer, M. (2019) “Evaluation of Regression Models: Model Assessment, Model Selection and Generalization Error”, Mach. Learn. Knowl. Extr. 1, 521–551.
[12]Gelb, A. (1974), Applied Optimal Estimation (4th Edition). Cambridge, Mass: MIT Press.
[13]Ostertagová, E. (2012), “Modelling Using Polynomial Regression”, Procedia Engineering, 48 (2012), pp. 500-506.
[14]Shearer, P.M. (1999), Introduction to Seismology, 1st edition Cambridge: Cambridge University Press.